Journal of Materials Chemistry A

PAPER

View Article Online
View Journal | View Issue



Cite this: J. Mater. Chem. A, 2014, 2, 18353

# Defect induced sodium disorder and ionic conduction mechanism in $Na_{1.82}Mg_{1.09}P_2O_7$†

Guandong Liu,[a] Shin-ichi Nishimura,[a] Sai Cheong Chung,[a] Kotaro Fujii,[b] Masatomo Yashima[b] and Atsuo Yamada*[a]

Received 1st July 2014
Accepted 30th August 2014

DOI: 10.1039/c4ta03356f

www.rsc.org/MaterialsA

Phase pure sodium magnesium pyrophosphate $Na_{1.82}Mg_{1.09}P_2O_7$ was synthesized by a solid state reaction, and used as a model system to understand the $Na^+$ dynamics in the related cathode materials $Na_{2-x}M_{1+x/2}P_2O_7$ (M = Fe, Mn, and Co). We found a three-dimensional framework structure formed by interconnecting $Mg_2O_{11}$ dimers with $P_2O_7$ pyrophosphate groups, where Na cages align along the [100] direction and are kinetically separated from each other. Diffuse distribution of Na was found inside the cage, and explained using a vacancy induced disorder model. Ionic conductivity is limited by inter-cage diffusion and measured to be $1.10 \times 10^{-11}$ S cm$^{-1}$ at room temperature with an activation energy of 0.77 eV. These features were further supported by bond-valence sum and lattice mechanics calculations.

## Introduction

Although lithium ion battery technology is still prominent as a high-energy density power source, future applications of secondary batteries will be much extended, thereby utilizing abundant elements becomes important. Sodium ion battery technology has attained renewed interest[1–3] especially for large scale applications, due to the natural abundance and low cost of Na.[4,5] Searching for earth-abundant new cathode materials, our group[6,7] and other researchers[8,9] have recently identified $Na_{2-x}Fe_{1+x/2}P_2O_7$ as a promising candidate with a moderate redox potential at 3 V *versus* $Na/Na^+$, a reasonable reversible capacity of about 100 mA h g$^{-1}$, and a good rate capability with 85% of its initial capacity retained even at a high rate of 5 C.[6]

As the high-rate capability requires superior transport properties, high ionic conductivity in the $Na_{2-x}M_{1+x/2}P_2O_7$ type of compounds is anticipated in general. Therefore, an understanding of their ionic conduction mechanism at the atomic scale is of interest based on the precise crystal structure. Redox activity can introduce undesirable structural imperfections into $Na_{2-x}M_{1+x/2}P_2O_7$ (M = transition metal), *i.e.* sodium non-stoichiometry and hole defects at the transition metal sites. In order to minimize these contributions to Na ion transport, we choose the redox-inactive Mg variant $Na_{2-x}Mg_{1+x/2}P_2O_7$ as a model system. Additionally, $Na_{2-x}Mg_{1+x/2}P_2O_7$ might be a good ionic conductor and a potential solid electrolyte.

In the 1970s, $Na_{2-x}Mg_{1+x/2}P_2O_7$ was initially designated as $Na_7Mg_{4.5}(P_2O_7)_4$ by Hanic *et al.*,[10,11] and its ionic conductivity was investigated by Znášik *et al.*[12] More recently, Erragh *et al.* reinvestigated the chemical composition, and concluded that $Na_{3.64}Mg_{2.18}(P_2O_7)_2$ ($Na_{1.82}Mg_{1.09}P_2O_7$) is the composition in the pure phase.[13] Most of the previous reports found deviations from the ideal stoichiometric $Na_2MP_2O_7$, and significant positional disorder at one Na site was observed. This kind of disordering is frequently found in good ionic conductors, as extended and shallow site potentials induce large thermal vibrations.

However, to the best of our knowledge, only glassy $Na_{1.82}Mg_{1.09}P_2O_7$ has been studied[14] before. The conductivity of a pure crystalline sample has never been obtained. In the present work, we succeeded in synthesizing a pure polycrystalline $Na_{1.82}Mg_{1.09}P_2O_7$ sample. The crystal structure and ionic conductivity at temperatures up to 773 K were investigated using synchrotron X-ray diffraction and AC impedance spectroscopy, followed by general discussions on the Na ionic diffusion mechanism in this type of structure with bond valence sum analysis and empirical force field calculation.

## Experimental section

### Material synthesis

$Na_{1.82}Mg_{1.09}P_2O_7$ was synthesized by a conventional solid-state method. Stoichiometric amounts of $NaH_2PO_4$ (Wako, 99%), $Mg(OH)_2$ (Wako, 99.9%), and $(NH_4)_2HPO_4$ (Wako, 99%) were mixed by planetary-type ball milling (400 rpm, 7 h). The mixture was then pressed into cylindrical pellets by a hand press, and calcined at 973 K for 12 h in an Ar atmosphere. After cooling to room temperature, pure white $Na_{1.82}Mg_{1.09}P_2O_7$ pellets were obtained.

[a]Department of Chemical System Engineering, The University of Tokyo, 7-3-1 Hongo, Bunkyo-ku, Tokyo 113-8656, Japan. E-mail: yamada@chemsys.t.u-tokyo.ac.jp

[b]Department of Chemistry and Materials Science, Graduate School of Science and Engineering, Tokyo Institute of Technology, 2-12-1-W4-17, O-okayama, Meguro-ku, Tokyo 152-8551, Japan

† Electronic supplementary information (ESI) available. See DOI: 10.1039/c4ta03356f

### Synchrotron powder X-ray diffraction

Synchrotron XRD was carried out at various temperatures ranging from room temperature to 773 K, on a multiple-detector system[15,16] at the BL4B2 station of Photon Factory, High Energy Accelerator Research Organization (KEK), Japan. The monochromatized X-ray wavelength was calibrated to be 1.196188 Å by measurement of SRM640c. The $2\theta$ step interval and range were 0.005° and 5–154° respectively. Rietveld refinement was performed using the TOPAS Version 3.0 or TOPAS-Academic Version 5 program, and the crystal structure and volumetric data were visualized by a computer program VESTA.[17]

### Impedance measurement

A powder sample was pressed into a cylindrical disk under 10 MPa, and then sintered at 973 K to maximize the density. Sizes of the sintered disks were typically 10 mm in diameter and 2 mm thick. The measured density was 2.25 g $cm^{-3}$, which corresponds to 79.2% of the theoretical value (2.84 g $cm^{-3}$). After that, both sides of the disk were coated with an Au film (500 nm in thickness) by a DC sputtering coater, and re-annealed at 773 K in an Ar atmosphere.

The AC impedance measurements were carried out with an SI 1260 Solartron impedance/gain-phase analyzer coupled to a 1296 dielectric interface. The scanning frequency range was 1 MHz to 0.01 Hz, and an applied AC voltage of 100 mV was used. The cylindrical disk was measured during heating from RT up to 773 K in a dry-air atmosphere. The step interval is set to 50 K, and the sample disk was held to equilibrate at each temperature for 1 h before measurements were started.

## Results and discussion

Synchrotron XRD patterns of $Na_{1.82}Mg_{1.09}P_2O_7$ at various temperatures are depicted in Fig. 1. All of the patterns demonstrate the triclinic lattice of $P\bar{1}$. Table 1 lists the lattice parameters at various temperatures, compared with the literature data.[13] The lattice parameters ($a$, $b$, $c$ and volume) increase linearly with temperature (Fig. 2). There is no anomalous feature in the diffraction patterns measured from room temperature to 773 K, except for continuous shifts of the peaks to lower angles due to thermal expansion of the unit cell, which proves that $Na_{1.82}Mg_{1.09}P_2O_7$ is thermally stable up to 773 K.

We used the structure model of Erragh *et al.*[13] as a starting point for the Rietveld refinement. Since the atomic scattering factors of $Na^+$ and $Mg^{2+}$ are almost identical due to the same electron number, X-ray diffraction is ineffective in deducing the accurate ratio of $Na^+/Mg^{2+}$. Thus, the total composition ratio of Na and Mg was fixed to the initial value (1.82 : 1.09). The final refinement patterns are shown in Fig. 1, and the detailed structure information is listed in Table S1† for the room temperature case. Some selected bond lengths and the bond valence sum (BVS) values of Mg and P at each site are listed in Table 2, which are consistent with the previous report.[13]

Fig. 3 depicts the crystal structure of $Na_{1.82}Mg_{1.09}P_2O_7$. There are four kinds of $PO_4$ tetrahedra, they connect in pairs to form diphosphates $P(1)O_3$–$O(4)$–$P(2)O_3$ and $P(3)O_3$–$O(11)$–$P(4)O_3$,

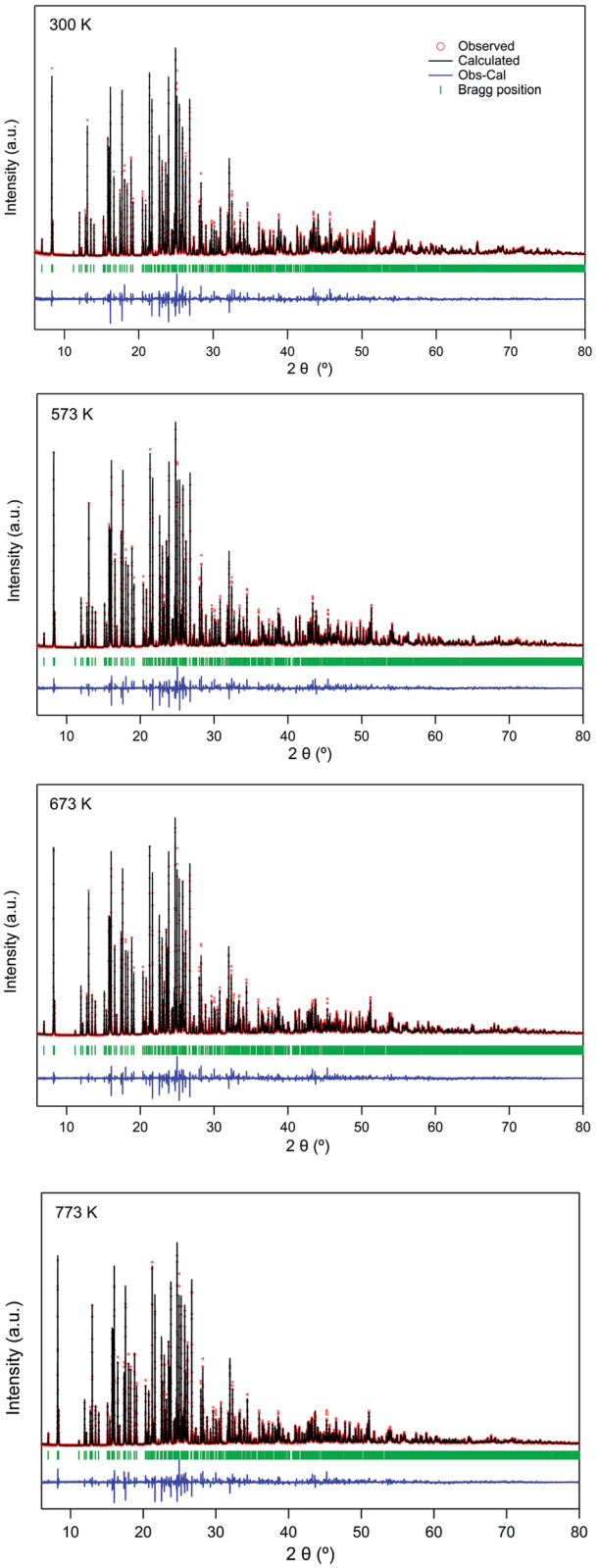


Fig. 1 Rietveld refinement patterns of synchrotron XRD of $Na_{1.82}Mg_{1.09}P_2O_7$ collected at 300 K ($R_p$ = 7.35%, $R_{wp}$ = 8.52%, and $\chi^2$ = 3.12); 573 K ($R_p$ = 6.70%, $R_{wp}$ = 7.91%, and $\chi^2$ = 3.55); 673 K ($R_p$ = 6.73%, $R_{wp}$ = 8.21%, and $\chi^2$ = 2.99); and 773 K ($R_p$ = 6.57%, $R_{wp}$ = 7.76%, and $\chi^2$ = 3.58).

Table 1 Lattice parameters of $Na_{1.82}Mg_{1.09}P_2O_7$ at various temperatures. The last row lists literature-reported data after standardization according to definite rules[29]

| Temperature (K) | $a$ (Å) | $b$ (Å) | $c$ (Å) | $\alpha$ (°) | $\beta$ (°) | $\gamma$ (°) | Volume (Å$^3$) |
|---|---|---|---|---|---|---|---|
| 300 | 6.39258(3) | 9.41968(4) | 10.90912(4) | 64.6804(2) | 80.2968(2) | 73.5798(2) | 568.720(4) |
| 573 | 6.41845(2) | 9.47593(3) | 10.95125(4) | 64.6881(2) | 80.3956(2) | 73.5067(2) | 576.548(3) |
| 673 | 6.42881(2) | 9.49758(3) | 10.96812(3) | 64.6926(2) | 80.4314(2) | 73.4797(2) | 579.657(3) |
| 773 | 6.43873(2) | 9.51873(3) | 10.98396(3) | 64.6996(2) | 80.4692(2) | 73.4519(2) | 582.663(3) |
| Room temp.[13] | 6.38200 | 9.40890 | 10.90100 | 64.7740 | 80.3600 | 73.6030 | 567.233 |

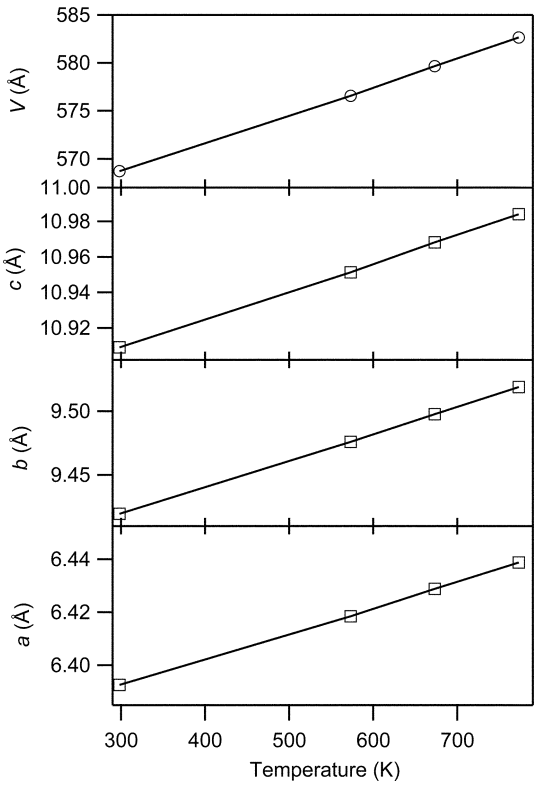


Fig. 2 Linear relationship of lattice parameters ($a$, $b$, $c$ and volume) to temperature in $Na_{1.82}Mg_{1.09}P_2O_7$.

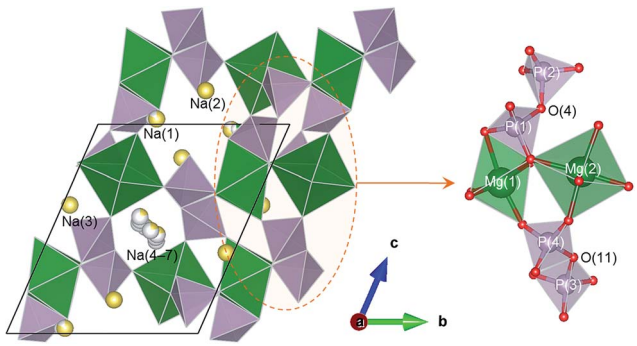


Fig. 3 Crystal structure of $Na_{1.82}Mg_{1.09}P_2O_7$. $MgO_6$ octahedra (green) and $PO_4$ (light purple) are interconnected to form the host structure, where Na (yellow) sites are located. The Na(1) site is a mixing site with Mg, the ratio of Na/Mg equals to 0.82/0.18; Na(4), Na(5), Na(6) and Na(7) sites are sub-sites for positional disorder.

where O(4) and O(11) are the bridging oxygen atoms. The bond angles for the bridging bond are 132.1° and 126.3° for P(1)–O(4)–P(2) and P(3)–O(11)–P(4), respectively. Mg atoms are located in two inequivalent octahedral sites, illustrated as $Mg(1)O_6$ and $Mg(2)O_6$. These magnesium octahedra are connected by corner sharing to form $Mg(1)Mg(2)O_{11}$ dimers. They tend to align along [010], and are interconnected by the $P_2O_7$ diphosphate groups. Specifically, the $P(3)O_3$–$O(11)$–$P(4)O_3$ groups interconnect $Mg(1)Mg(2)O_{11}$ dimers by only corner

Table 2 Selected bond lengths (Å) and bond valence sum (BVS) values for $Na_{1.82}Mg_{1.09}P_2O_7$

| | | | |
|---|---|---|---|
| P(1)–P(4) = 1.595(7) | P(2)–O(1) = 1.523(6) | P(3)–O(11) = 1.648(6) | P(4)–O(8) = 1.513(7) |
| P(1)–P(5) = 1.524(6) | P(2)–O(2) = 1.509(6) | P(3)–O(12) = 1.537(7) | P(4)–O(9) = 1.532(7) |
| P(1)–P(6) = 1.525(7) | P(2)–O(3) = 1.525(7) | P(3)–O(13) = 1.500(7) | P(4)–O(10) = 1.510(7) |
| P(1)–P(7) = 1.522(7) | P(2)–O(4) = 1.619(6) | P(3)–O(14) = 1.510(7) | P(4)–O(11) = 1.637(7) |
| ⟨P(1)–O⟩ = 1.5413 | ⟨P(2)–O⟩ = 1.5439 | ⟨P(3)–O⟩ = 1.5488 | ⟨P(4)–O⟩ = 1.5477 |
| BVS = 4.924 | BVS = 4.906 | BVS = 4.867 | BVS = 4.870 |

| | |
|---|---|
| Mg(1)–O(6) = 2.201(7) | Mg(2)–O(2) = 2.011(6) |
| Mg(1)–O(7) = 2.280(7) | Mg(2)–O(3) = 2.110(5) |
| Mg(1)–O(8) = 1.965(7) | Mg(2)–O(5) = 2.128(7) |
| Mg(1)–O(9) = 1.989(7) | Mg(2)–O(6) = 2.171(7) |
| Mg(1)–O(13) = 1.960(7) | Mg(2)–O(10) = 2.100(6) |
| Mg(1)–O(1) = 2.051(7) | Mg(2)–O(12) = 2.071(6) |
| ⟨M(1)–O⟩ = 2.0744 | ⟨M(2)–O⟩ = 2.0983 |
| BVS = 2.253 | BVS = 2.025 |

sharing, whereas the $P(1)O_3$–$O(4)$–$P(2)O_3$ groups do so by both corner and edge sharing.

Interconnections of $Mg_2O_{11}$ and $P_2O_7$ dimers build a 3-D framework, where Na atoms are situated. There are 4 crystallographic Na sites: Na(1) with substitutional disorder ($Mg_{Na}^{+}$), Na(2) and Na(3) with full occupancies, and a positional disordered site Na(4). In the Rietveld refinement, we introduced two modifications to the starting model:[13] (1) removal of the positional restriction at Na(1), (2) using a site splitting model with 4 Na sub-sites for Na(4), instead of 3 in the original model. The split-atom sites are now designated as Na(4)/Na(5)/Na(6)/Na(7). Initial refinement found that occupancies of the 4 split-atom sites are similar so we used an equal occupancy of 0.205 at each site in subsequent refinements. To justify the positional disordering, we performed a difference Fourier analysis between observed peaks and intensities deduced from structural models with and without Na occupying the original Na(4) site. Fig. 4 shows the difference Fourier map results. The density shows a diffuse distribution as expected from our model and previous studies.[13] These modifications decreased $R$ values for Rietveld refinement significantly (ESI Fig. S1†).

The temperature-dependent conductivity is shown in Fig. 5. A Nyquist plot measured at 533 K is depicted in the inset as an example. An obvious Warburg tail at low frequency indicates the capacitance of blocking electrodes. This is typical behavior of

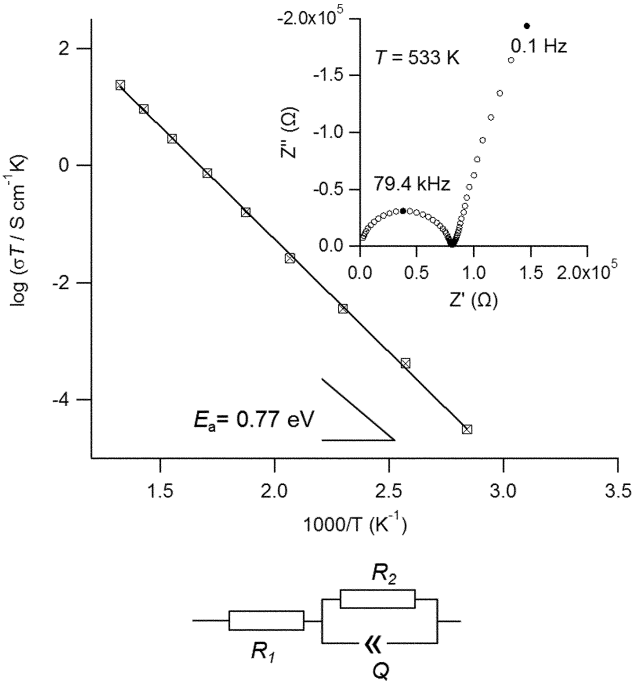


Fig. 5 Arrhenius plot $\log(\sigma T)$ *versus* $1000/T$ in $Na_{1.82}Mg_{1.09}P_2O_7$. The inset is the Nyquist plot at 533 K.

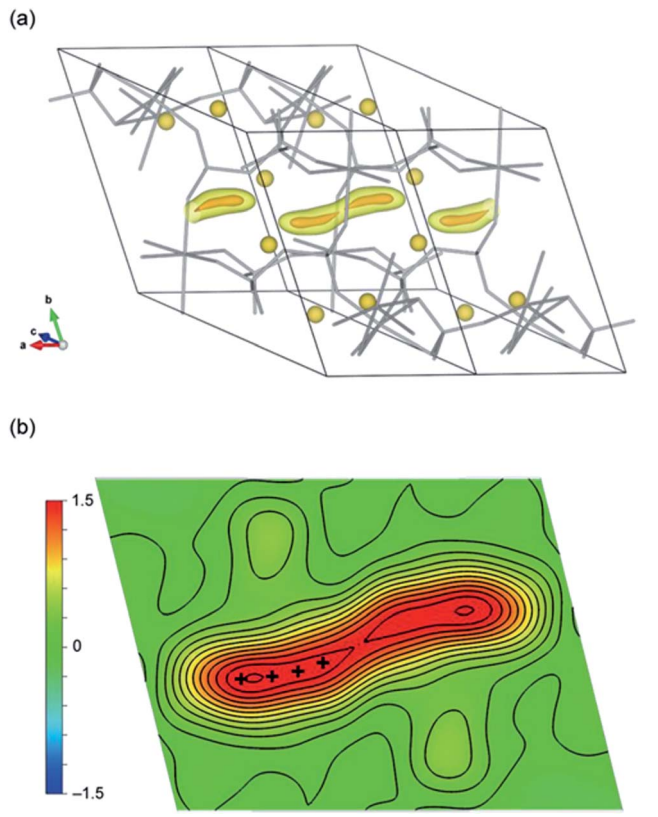


Fig. 4 (a) Difference Fourier map from structure models with and without Na in the positional disordered sites and its across-sectional plane around the Na cage (b). The symbol + indicates the positions of sub-sites Na(4)/Na(5)/Na(6)/Na(7).

ionic conductors with ionic blocking electrodes. The depressed semi-circle part at high frequency can be fitted by an $R_1(R_2Q)$ equivalent circuit, where $R_1$ represents the shift of an initial point of impedance arc from zero, and can be assigned to the contact resistance of the sample with electrodes, $R_2$ is the sum of the grain boundary and bulk resistances, and $Q$ is the constant phase element (CPE), indicating the properties of the sample, *i.e.* homogeneity. The resistance of the sample $R$ equals to $R_1 + R_2$. Variation of the conductivity with temperature is shown in Fig. 5, it is fitted to the Arrhenius expression, $\sigma T = \sigma_0 \exp(-E_a/k_BT)$, where $\sigma_0$ is a pre-exponential factor, $E_a$ is the activation energy, and $k_B$ is the Boltzmann constant. An activation energy of 0.77 eV is deduced.

Table 3 summarizes our activation energy and ionic conductivity at 573 K compared with related values in the literature. Our sample shows comparable values with the glassy sample reported by Dridi *et al.*,[14] but distinguished from the reported $Na_7Mg_{4.5}(P_2O_7)_4$ samples[12] which gives a much higher activation energy (>1 eV). However, even our sample shows a higher conductivity at 573 K and lower activation energy than that of the previous reports, its conduction properties are still not so impressive.

To understand the reason for the limited conductivity, a closer look at the structure analysis is necessary. The temperature dependences of the atomic displacement parameters of Na are shown in Fig. 6. The Na(1) site shows significantly lower atomic thermal parameters than those at Na(2) and Na(3) sites, as substituted Mg lowers the atomic displacement at Na(1). The refinement of each $B$ value for sub-sites Na(4)/Na(5)/Na(6)/Na(7) failed due to significant overlaps of displacement among these sites. Instead, a uniform value was used for these sub-sites to

 

Table 3 Ionic conductivity and activation energy of $Na_{1.82}Mg_{1.09}P_2O_7$

| Sample | $\sigma_{573\ K}$ (S cm$^{-1}$) | $E_a$ (eV) | Reference |
|---|---|---|---|
| $Na_7Mg_{4.5}(P_2O_7)_4$ (crystalline) | $3.89 \times 10^{-7}$ | 1.115 | P. Znášik *et al.*[12] |
| $Na_7Mg_{4.5}(P_2O_7)_4$ (glassy) | $2.11 \times 10^{-6}$ | 0.995 | P. Znášik *et al.* |
| $Na_{1.82}Mg_{1.09}P_2O_7$ (glassy) | $8.91 \times 10^{-6}$ | 0.85 | N. Dridi *et al.*[14] |
| $Na_{1.82}Mg_{1.09}P_2O_7$ (crystalline) | $9.30 \times 10^{-6}$ | 0.77 | This work |

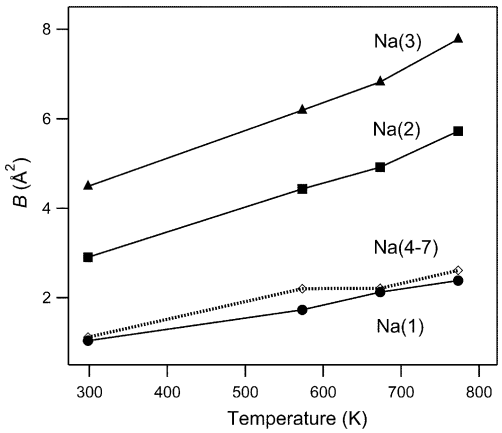


Fig. 6 Temperature dependence of atomic displacement parameters of Na.

detect its temperature dependence. The obtained average $B$ value in the cage (Na(4)/Na(5)/Na(6)/Na(7)) varies from 1.12 to 2.61 Å$^2$ in the temperature range of 300–773 K, showing a similar temperature sensitivity to that at the Na(1) site (Fig. 6). The temperature-insensitive $B$ value indicates that the positional disorder at Na(4)/Na(5)/Na(6)/Na(7) sub-sites may be static. If this assumption applies, the diffuse distribution in the Na cage (Fig. 4) is actually a result of a superposition of local displacements.

The static disorder hypothesis can be understood by a vacancy induced disorder model shown in Fig. 7. With a defect free and ideal composition, $Na_2MgP_2O_7$ should have a well ordered Na arrangement, in which the Na ions are located at one-side of the anisotropic cage due to an intra-cage Na–Na

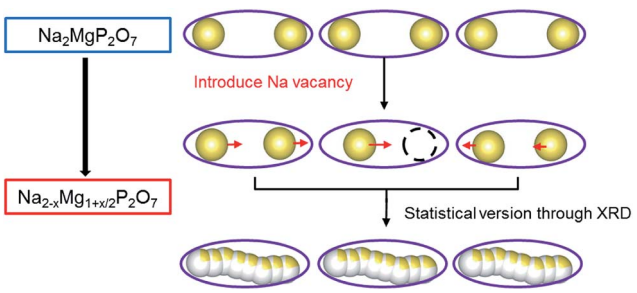


Fig. 7 Schematic of positional disorder formation in the Na cage. Purple circles represent the Na cages embraced by a 3D framework structure.

electrostatic repulsion. On the other hand, the present composition contains 18% of Na vacancies in the Na cage. The vacancy induces large intra-cage displacement toward the lowest-energy position in the cage, and simultaneously causes displacements of Na ions in adjacent Na cages. Superimposing these displacements over the whole crystal leads to the diffuse Na distribution in the Na cage.

In order to quantify the Na site potential, we calculated the bond valence sum (BVS) map for Na in the present anion framework. The BVS calculation has been successfully applied to model ion diffusion pathways in various compounds,[18–20] the bond valence of each ionic pair $s_{ij}$ is calculated as:

$$s_{ij} = \exp[(R_0 - R_{ij})/b] \quad (1)$$

where $R_0$ and $b$ are tabulated empirical parameters[21] and equal to 1.803 and 0.37 in this work, respectively; $R_{ij}$ represents the bond length of Na($i$)–O($j$). The sum of the bond valence for each site $i$ gives the BVS value:

$$V_i = \sum_j s_{ij} \quad (2)$$

The difference of $V_i$ from the ideal valence $V_{ideal}$

$$|\Delta V| = |V_i - V_{ideal}| \quad (3)$$

gives a standard of positional suitability for Na ions. We calculated $|\Delta V|$ in the whole space of the unit cell with a grid size of 0.2 × 0.2 × 0.2 Å$^3$. Smaller $|\Delta V|$ values correspond to stable positions for Na, and the connections among these points indicate possible Na diffusion paths. In contrast, the positions with high $|\Delta V|$ values are associated with bottlenecks for Na ion diffusion.

Fig. 8 shows two isosurfaces with $|\Delta V| = 0.1$ (pink) and 0.3 (green), respectively. They enclose the region with $|\Delta V|$ lower than the specified values. The pink isosurface ($|\Delta V| = 0.1$) distributes exclusively in the separated regions around the Na(2) and Na(3) sites, confirming the stability of these sites. Na(1) and sub-sites Na(4)/Na(5)/Na(6)/Na(7) have slightly higher $|\Delta V|$ values, compatible with the fact that substitutional disorder and static displacement exist. Within the isosurface where $|\Delta V| = 0.3$, the Na cage [Na(7)/Na(6)/Na(5)/Na(4)/Na(4)/Na(5)/Na(6)/Na(7)] is enclosed (Fig. 8). However, this isosurface is interrupted between the neighbor cages. It highlights that migration bottlenecks exist between neighboring Na cages along [100]. These bottlenecks impede Na ion conductivity, and vetoes high ionic diffusion in $Na_{1.82}Mg_{1.09}P_2O_7$, although high mobility of Na within the cage is possible. Besides, the Na cage

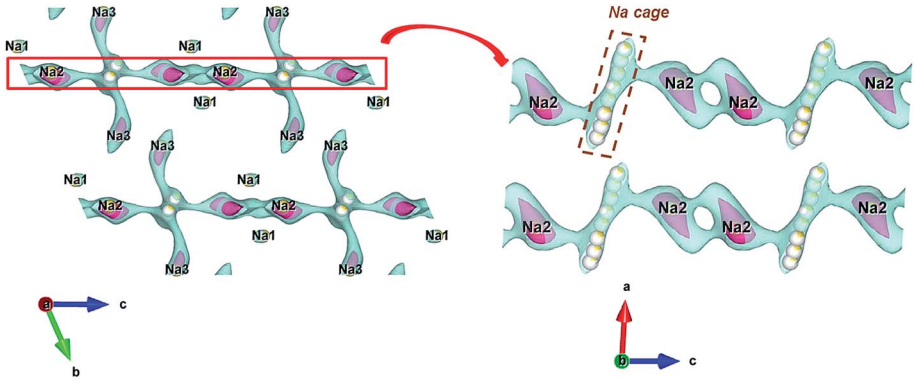


Fig. 8 Isosurface of bond valence sum deviation ($|\Delta V|$) for Na in $Na_{1.82}Mg_{1.09}P_2O_7$, based on the structure at room temperature. $|\Delta V|$ is 0.3 on the green isosurface, and 0.1 on the pink isosurface.

and Na(2) (or Na(3)) sites are enclosed within the isosurface with $|\Delta V| = 0.3$ (Fig. 8), indicating that between them there can be possible Na diffusion channels.

Since BVS calculation only considers the effects from anions ($O^{2-}$), and ignores the interaction between cations, it is inadequate for fully elucidating the Na diffusion mechanism. Therefore empirical force field calculation was applied. Energy barriers for each Na migration path were calculated by the lattice mechanics calculation package GULP.[22] The Buckingham-type potential was used for two body interactions. The three-body spring constant was used for bond angle restrictions of the phosphate group. To model the charge polarization, the shell model was used for the oxygen atoms. And the nudged elastic band (NEB) method was used to model the transition state.

Fig. 9 shows the calculated energy barriers for Na migration between adjacent sites. The Na(1) site was excluded due to two reasons: (1) our BVS calculation results show that the Na(1) site has a slightly higher $|\Delta V|$ value ($\approx$0.22), and therefore is unfavorable for Na to migrate in, (2) the substitutional ion ($Mg^{2+}$) at the Na(1) site has a higher valence, this usually shows a "blocking" effect to ion diffusion, similar phenomena have already been observed in phosphates,[23,24] silicates[25,26] and fluorosulfates.[27]

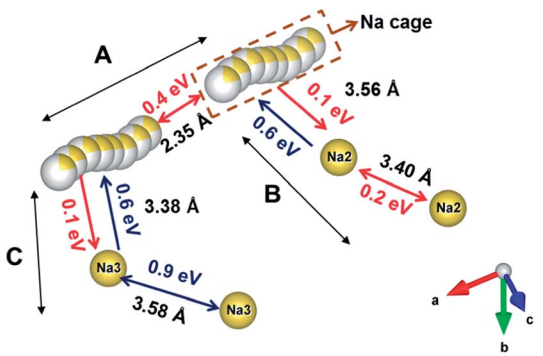


Fig. 9 Migration energy barriers and related distances between adjacent Na sites.

Three possible Na migration paths were examined, and are described in Fig. 9. Path A is between the adjacent Na cages, and aligns along [100] with the shortest jump distance of 2.35 Å. Path B is parallel to the [001] direction and involves the migrations in a sequence of the Na cage/Na(2)/Na(2)/Na cage (Fig. 9), with jump distances of 3.40–3.56 Å. Path C represents the migration between the Na cage and Na(3) site along [010], having a jump distance of 3.38 Å.

Path A shows the lowest Na migration energy of 0.4 eV and the shortest jump distance, therefore, it is the favorite path for Na ion diffusion. Along the paths of B and C, the migration barriers are largely asymmetric: 0.1 eV for the direction from the Na cage to Na(2) or Na(3), and *ca.* 0.6 eV for the opposite direction. This is due to different defect formation energies for the each site. Defect in the Na cage is more stable than in Na(2) and Na(3) sites by *ca.* 0.5 eV, thus the migration of Na ions to the Na cage from the Na(2) or Na(3) site is unfavorable.

Even though the paths of B and C need slightly higher migration energies and longer jump distances, they are not so distinguished from that of the lowest energy path (path A). In contrast, in olivine-type $LiFePO_4$, Li migration along the *b* axis shows a significantly lower activation energy (0.55 eV) than those along the other directions (>2.8 eV),[23] and a one dimensional ion diffusion mechanism is concluded. Thus, $Na_{1.82}Mg_{1.09}P_2O_7$ may be classified as an ionic conductor with three dimensional diffusion channels. Additionally, in our previous work[7] we found that nearly one Na per formula unit can be extracted from $Na_{2-x}Fe_{1+x/2}P_2O_7$. It shows that beside the Na ions in the Na cage, both Na(2) and Na (3) sites can be accessed electrochemically, confirming the existence of 3-D Na ion diffusion paths in this structure type.

Finally, we should point out the limit of using $Na_{2-x}Mg_{1+x/2}P_2O_7$ to model the $Na_{2-x}Fe_{1+x/2}P_2O_7$ system. In Fig. S2† we compare the BVS map of these two compounds. Connecting the favorable migration path along Na cages needs a BVS isosurface with $|\Delta V| \geq 0.4$ for $Na_{2-x}Fe_{1+x/2}P_2O_7$, but $|\Delta V| \geq 0.6$ for $Na_{1.82}Mg_{1.09}P_2O_7$. Therefore, one expects that Na migration needs a lower activation energy for $Na_{2-x}Fe_{1+x/2}P_2O_7$. The bottleneck for Na migration along the favorable path consists of two $P_2O_7$ dimers separated by $MO_6$ (M = Fe and Mg) octahedra (Fig. S2†). The average length of the Fe–O

 

bonds (~2.16 Å) is longer than the Mg–O bonds (~2.10 Å), and this bond length difference accounts for ~0.1–0.2 Å difference in the size of the bottleneck. Consequently, the ionic conductivity of $Na_{2-x}Fe_{1+x/2}P_2O_7$ is expected to be higher than that of $Na_{1.82}Mg_{1.09}P_2O_7$. A recent theoretical study by Clark *et al.*[28] shows that Na ion diffusion in $Na_2FeP_2O_7$ is of 3 dimensional nature. The calculated lowest energy migration path is along path A and has a value of 0.33 eV. These are consistent with our conclusions. They also indicated that the low activation energy for Na transport in $Na_2FeP_2O_7$ is one of the reasons for its high rate capability as a Na-based cathode material.

## Conclusion

In summary, nonstoichiometric $Na_{1.82}Mg_{1.09}P_2O_7$ has been synthesized by the solid state method in the present work. The crystal structure and ionic conductivity have been investigated in a wide temperature range (300–773 K). With bond valance sum and empirical force field calculations, the Na migration mechanism has been elaborated. The main results are listed as follows:

(1) Highly positional disorder of Na was observed at sub-sites Na(4)/Na(5)/Na(6)/Na(7), which consist of Na cages aligning along [100]. The average atomic thermal parameter at Na(4)/Na(5)/Na(6)/Na(7) shows weak temperature dependence. It indicates static disorder inside the Na cages, and a vacancy induced disorder model was proposed.

(2) The ionic conductivity of the crystalline $Na_{1.82}Mg_{1.09}P_2O_7$ sample has been reported for the first time, which equals to $9.30 \times 10^{-6}$ S cm$^{-1}$ at 573 K. The activation energy is 0.77 eV, consistent with previous work on a glassy sample. Using the Arrhenius equation, a room-temperature ionic conductivity of $1.10 \times 10^{-11}$ S cm$^{-1}$ was also obtained.

(3) Based on empirical force field calculation, 3D Na diffusion channels in this type of structure have been proven. Specifically, the migration along Na cages [Na(7)/Na(6)/Na(5)/Na(4)/Na(4)/Na(5)/Na(6)/Na(7)] has been found to be the favorite path for Na migration. However, the BVS map reveals that bottlenecks exist between neighbor cages which impede Na ion migration, despite the highly favorable positional disorder of Na within the cages.

(4) The Na migration mechanism can shed light on other isostructural $Na_{2-x}M_{1+x/2}P_2O_7$-type compounds, *i.e.* $Na_{2-x}Fe_{1+x/2}P_2O_7$, one promising cathode material for Na ion batteries.

## Acknowledgements

The present work was performed under a management of "Elements Strategy Initiative for Catalysts and Batteries" (ESICB) project supported by Ministry of Education Culture, Sports, Science and Technology, Japan. The synchrotron radiation experiment was performed under the approval of the Photon Factory Program Advisory Committee (Proposal No. 2013G670, 2011G683).

## References

1 S.-W. Kim, D.-H. Seo, X. Ma, G. Ceder and K. Kang, *Adv. Energy Mater.*, 2012, **2**, 710–721.
2 B. L. Ellis and L. F. Nazar, *Curr. Opin. Solid State Mater. Sci.*, 2012, **16**, 168–177.
3 V. Palomares, P. Serras, I. Villaluenga, K. B. Hueso, J. Carretero-González and T. Rojo, *Energy Environ. Sci.*, 2012, **5**, 5884–5901.
4 C. Grosjean, P. H. Miranda, M. Perrin and P. Poggi, *Renewable Sustainable Energy Rev.*, 2012, **16**, 1735–1744.
5 D. Poole, B. B. Argent, V. N. Sharifi and J. Swithenbank, *Fuel*, 2008, **87**, 1318–1333.
6 P. Barpanda, T. Ye, S. Nishimura, S.-C. Chung, Y. Yamada, M. Okubo, H. Zhou and A. Yamada, *Electrochem. Commun.*, 2012, **24**, 116–119.
7 P. Barpanda, G. Liu, C. D. Ling, M. Tamaru, M. Avdeev, S.-C. Chung, Y. Yamada and A. Yamada, *Chem. Mater.*, 2013, **25**, 3480–3487.
8 H. Kim, R. A. Shakoor, C. Park, S. Y. Lim, J.-S. Kim, Y. N. Jo, W. Cho, K. Miyasaka, R. Kahraman, Y. Jung and J. W. Choi, *Adv. Funct. Mater.*, 2013, **23**, 1147–1155.
9 K.-H. Ha, S. H. Woo, D. Mok, N.-S. Choi, Y. Park, S. M. Oh, Y. Kim, J. Kim, J. Lee, L. F. Nazar and K. T. Lee, *Adv. Energy Mater.*, 2013, **3**, 770–776.
10 J. Majling and F. Hanic, *J. Solid State Chem.*, 1973, **7**, 370–373.
11 F. Hanic and Z. Zak, *J. Solid State Chem.*, 1974, **10**, 12–19.
12 P. Znášik, I. Hinduliakova and J. Majlin, *Solid State Ionics*, 1993, **60**, 313–317.
13 F. Erragh, A. Boukhari, F. Abraham and B. Elouadi, *J. Solid State Chem.*, 2000, **152**, 323–331.
14 N. Dridi, A. Boukhari and J. M. Reau, *Solid State Ionics*, 1998, **110**, 131–136.
15 H. Toraya, H. Hibino and K. Ohsumi, *J. Synchrotron Radiat.*, 1996, **3**, 75–83.
16 (*a*) M. Yashima, M. Tanaka, K. Oh-uchi and T. Ida, *J. Appl. Crystallogr.*, 2005, **38**, 854–855; (*b*) M. Yashima, K. Oh-uchi, M. Tanaka and T. Ida, *J. Am. Ceram. Soc.*, 2006, **89**, 1395–1399.
17 K. Momma and F. Izumi, *J. Appl. Crystallogr.*, 2011, **44**, 1272–1276.
18 S. Adams, *Solid State Ionics*, 2000, **136–137**, 1351–1361.
19 D. Mazza, *J. Solid State Chem.*, 2001, **156**, 154–160.
20 M. Avdeev, M. Sale, S. Adams and R. P. Rao, *Solid State Ionics*, 2012, **225**, 43–46.
21 I. D. Brown and D. Altermatt, *Acta Crystallogr., Sect. B: Struct. Sci.*, 1985, **41**, 244–247.
22 J. Gale, *J. Chem.Soc., Faraday Trans.*, 1997, **93**, 629–637.
23 M. S. Islam, D. J. Driscoll, C. A. J. Fisher and P. R. Slater, *Chem. Mater.*, 2005, **17**, 5085–5092.
24 C. Fisher, V. H. Prieto and M. Islam, *Chem. Mater.*, 2008, **20**, 5907–5915.
25 N. Kuganathan and M. S. Islam, *Chem. Mater.*, 2009, **21**, 5196–5202.
26 A. R. Armstrong, N. Kuganathan, M. S. Islam and P. G. Bruce, *J. Am. Chem. Soc.*, 2011, **133**, 13031–13035.
27 R. Tripathi and G. Gardiner, *Chem. Mater.*, 2011, **23**, 2278–2284.
28 J. M. Clark, P. Barpanda, A. Yamada and M. S. Islam, *J. Mater. Chem. A*, 2014, **2**, 11807–11812.
29 E. Parthé and L. M. Gelato, *Acta Crystallogr., Sect. B: Struct. Sci.*, 1984, **A40**, 169–183.